J|A|C|S ARTICLES

Published on Web 09/16/2009

Structure Sensitivity of Methanol Electrooxidation on Transition Metals

Peter Ferrin and Manos Mavrikakis*

Department of Chemical and Biological Engineering, University of Wisconsin-Madison, 1415 Engineering Drive, Madison, Wisconsin 53706

Received May 21, 2009; E-mail: manos@engr.wisc.edu

Abstract: We have investigated the structure sensitivity of methanol electrooxidation on eight transition metals (Au, Ag, Cu, Pt, Pd, Ir, Rh, and Ni) using periodic, self-consistent density functional theory (DFT-GGA). Using the adsorption energies of 16 intermediates on two different facets of these eight face-centered-cubic transition metals, combined with a simple electrochemical model, we address the differences in the reaction mechanism between the (111) and (100) facets of these metals. We investigate two separate mechanisms for methanol electrooxidation: one going through a CO* intermediate (the indirect pathway) and another that oxidizes methanol directly to CO_2 without CO* as an intermediate (the direct pathway). A comparison of our results for the (111) and (100) surfaces explains the origin of methanol electrooxidation's experimentally-established structure sensitivity on Pt surfaces. For most metals studied, on both the (111) and (100) facets, we predict that the indirect mechanism has a higher onset potential than the direct mechanism. Ni(111), Au(100), and Au(111) are the cases where the direct and indirect mechanisms have the same onset potential. For the direct mechanism, Rh, Ir, and Ni show a lower onset potential on the (111) facet, whereas Pt, Cu, Ag, and Au possess lower onset potential on the (100) facet. Pd(100) and Pd(111) have the same onset potential for the direct mechanism. These results can be rationalized by the stronger binding energy of adsorbates on the (100) facet versus the (111) facet. Using linear scaling relations, we establish reactivity descriptors for the (100) surface similar to those recently developed for the (111) surface; the free energies of adsorbed CO* and OH* can describe methanol electrooxidation trends on various metal surfaces reasonably well.

Introduction

Direct methanol fuel cells (DMFCs) are attracting considerable attention, especially in the area of portable-power applications.[1,2] Many of the problems present in hydrogen PEM fuel-cell technology, particularly those concerning hydrogen storage, can be circumvented by using methanol as a fuel.[3] However, certain technical challenges, such as their low activity and efficiency as compared to H_2-PEM fuel cells, limit the usefulness of DMFCs.[4] Specifically, regarding electrocatalysis at the DMFC anode, there are two related concerns: (1) CO is a very stable intermediate resulting from methanol decomposition while simultaneously being a strong poison for the platinum electrode and thus seriously reducing its activity;[4] and (2) the anode overpotential with existing technology is higher than that of a hydrogen-based fuel cell, thus reducing the overall fuel cell efficiency, even though the equilibrium potential of the anode reaction is similar to that of the hydrogen fuel cell anode.

To solve these problems, various groups have proposed modifying the anode catalyst.[3] While Pt is the transition metal with the highest activity for this reaction, it does not have adequate electrooxidation activity at practically relevant overpotentials.[4] Several alloy catalysts (especially the well-known Pt−Ru alloy[4−6] and its derivatives[7,8]) have been proposed to lower the working overpotential and increase the activity of DMFC anodes through a combination of bifunctional[9] and ligand[10,11] effects. However, there is still room for improvement in catalyst design for two main reasons: (1) even with these new materials, activity and efficiency are lower than desired, and (2) most of these alloys are composed of very expensive transition metals, and therefore the cost is prohibitive, particularly for large-scale applications.

Density functional theory (DFT) has been used to better understand many aspects of electrochemical reactions. For instance, DFT has been implemented for elucidating the

(1) Cooper, H. *Chem. Eng. Prog.* **2007**, *103*, 34.
(2) Dillon, R.; Srinivasan, S.; Arico, A. S.; Antonucci, V. *J. Power Sources* **2004**, *127*, 112.
(3) Liu, H. S.; Song, C. J.; Zhang, L.; Zhang, J. J.; Wang, H. J.; Wilkinson, D. P. *J. Power Sources* **2006**, *155*, 95.
(4) Jarvi, T. D.; Stuve, E. M. Fundamental Aspects of Vacuum and Electrocatalytic Reactions of Methanol and Formic Acid on Platinum Surfaces. In *The Science of Electrocatalysis on Bimetallic Surfaces*; Lipkowski, J., Ross, P., Eds.; Wiley-VCH, Inc.: New York, 1998; p 75.
(5) Reddington, E.; Sapienza, A.; Gurau, B.; Viswanathan, R.; Sarangapani, S.; Smotkin, E. S.; Mallouk, T. E. *Science* **1998**, *280*, 1735.
(6) Petrii, O. A. *J. Solid State Electrochem.* **2008**, *12*, 609.
(7) Gurau, B.; Viswanathan, R.; Liu, R. X.; Lafrenz, T. J.; Ley, K. L.; Smotkin, E. S.; Reddington, E.; Sapienza, A.; Chan, B. C.; Mallouk, T. E.; Sarangapani, S. *J. Phys. Chem. B* **1998**, *102*, 9997.
(8) Lima, A.; Coutanceau, C.; Leger, J. M.; Lamy, C. *J. Appl. Electrochem.* **2001**, *31*, 379.
(9) Watanabe, M.; Motoo, S. *J. Electroanal. Chem.* **1975**, *60*, 275.
(10) Frelink, T.; Visscher, W.; Vanveen, J. A. R. *Surf. Sci.* **1995**, *335*, 353.
(11) Greeley, J.; Mavrikakis, M. *Catal. Today* **2006**, *111*, 52.

mechanisms for the oxygen reduction reaction,[12,13] the hydrogen evolution reaction,[14] electrochemical water splitting,[15] and methanol electrooxidation.[16,17] On the basis of this understanding, one can identify essential characteristics for good electrocatalysts; this approach has been successful in identifying new materials for potential application as electrocatalysts.[18,19] In addition, DFT has been used to describe other relevant electrochemical phenomena such as metal dissolution.[20,21]

To identify better catalysts for use as DMFC anodes, it is important to understand the mechanism of methanol electrooxidation on the catalyst surface. Recent work details a model of this reaction using two "reactivity descriptors", the adsorption energies of carbon monoxide and hydroxyl, to predict the lowest potential at which methanol electrooxidation can occur on close-packed (111) and (0001) transition metal surfaces.[17] Additionally, this model allows for the prediction of the methanol electrooxidation pathway at low potentials on those surfaces. However, there is evidence that methanol electrooxidation may be structure sensitive.[16,22−24] Particle size effects have been previously reported on supported Pt nanocatalysts for this reaction.[25,26] In single-crystal studies, higher currents at a given potential for the Pt(100) surface as compared to the Pt(111) surface have been reported at intermediate potentials.[23] Additionally, several groups have reported a difference in both the mechanism of electrooxidation and the extent of CO* poisoning on Pt(100) and Pt(111).[16,22,23]

In this work, we develop a model for methanol electrooxidation on the (100) facets of eight fcc metals and contrast it with that on the (111) facets of the same metals. Using this framework, we elucidate the reasons for the structure sensitivity of this reaction established on pure Pt. We then make predictions as to the structure sensitivity of this reaction on seven other fcc transition metals, where only limited systematic experimental electrocatalytic studies could be found. Subsequently, we generalize our findings by characterizing the onset potential (that is, the potential at which the reaction is downhill in free energy) of a general fcc(100) surface using two parameters: the free energies of adsorbed carbon monoxide and hydroxyl species, respectively. Finally, we suggest how our results can offer some guidance toward the identification of improved DMFC anode alloy catalysts.

Methods

The adsorption energetics of all adsorbates are calculated using DFT as implemented through DACAPO, a total energy code.[27,28] A periodic 3 × 3 surface unit cell (corresponding to a 1/9 ML coverage for each adsorbate) of the fcc(100) surface with four layers of metal atoms and five equivalent vacuum layers between successive slabs is used in this study. Adsorption is allowed on only one of the two exposed surfaces, with the dipole moment adjusted accordingly.[29,30] The bottom two layers of metal atoms in each slab are kept fixed at their bulk positions, while the top two layers are allowed to relax. Adding more layers of metal atoms and allowing further relaxation showed a negligible effect on adsorbate binding energies. Ionic cores are described by Vanderbilt ultrasoft pseudopotentials.[31] The Kohn−Sham one-electron sets are expanded in a series of plane waves with a kinetic energy cutoff of 25 Ry. The surface Brillouin zone is sampled using a Monkhorst−Pack 4 × 4 × 1 grid.[32] The exchange-correlation energy is described by the self-consistent Perdew−Wang generalized gradient approximation (PW91-GGA).[33] Electron density is determined through the iterative diagonalization of the Kohn−Sham Hamiltonian, Fermi population of the Kohn−Sham states (k_BT = 0.1 eV), and Pulay mixing of the resulting electron density. All total energies have been extrapolated to 0 K. The energetics determined here are sufficiently accurate to determine trends for methanol electrooxidation across the periodic table. Calculations involving Ni are spin polarized. To account for zero-point energy, we calculate vibrational frequencies of gas-phase molecules and adsorbates on Pt by numerical differentiation of forces implementing a second-order finite difference approach with a step-size of 0.015 Å.[34] The Hessian matrix is mass-weighted and diagonalized to yield the frequencies and normal modes of vibration for the adsorbed species. We assume that the zero-point energies and entropies of adsorbates on other metals are similar to that of Pt. Prior work has shown that this assumption is fairly accurate.[12,17]

We also account for changes in entropy. For gas- and liquid-phase molecules, tabulated values of entropy from the literature are used.[35] For molecules bound to the surface, the vibrational entropy is calculated assuming a quantum mechanical harmonic oscillator with the same vibrational frequencies as for the zero-point energy.

All free energies are calculated relative to H_2O, CO_2, and H_2; for example, the free energy of methanol is calculated from the reaction

$$CO_2(g) + 3H_2(g) \rightarrow CH_3OH(g) + H_2O(1)$$

as follows:

$$\Delta G_{CH3OH} = TE_{H2O} + TE_{CH3OH} - TE_{CO2} - 3{*}TE_{H2} + ZPE_{H2O} + ZPE_{CH3OH} - ZPE_{CO2} - 3{*}ZPE_{H2} - T{*}(S_{H2O} + S_{CH3OH} - 3{*}S_{H2} - S_{CO2})$$

where *TE* is the total energy of reactant and product species calculated by DFT, *T* is the standard temperature (298 K), *ZPE* is the zero-point energy for the species as calculated from the vibrational frequencies, and *S* is the entropy of the species. Free

(12) Nørskov, J. K.; Rossmeisl, J.; Logadottir, A.; Lindqvist, L.; Kitchin, J. R.; Bligaard, T.; Jonsson, H. *J. Phys. Chem. B* **2004**, *108*, 17886.
(13) Nilekar, A. U.; Mavrikakis, M. *Surf. Sci.* **2008**, *602*, L89.
(14) Greeley, J.; Nørskov, J. K.; Kibler, L. A.; El-Aziz, A. M.; Kolb, D. M. *ChemPhysChem* **2006**, *7*, 1032.
(15) Rossmeisl, J.; Dimitrievski, K.; Siegbahn, P.; Nørskov, J. K. *J. Phys. Chem. C* **2007**, *111*, 18821.
(16) Cao, D.; Lu, G. Q.; Wieckowski, A.; Wasileski, S. A.; Neurock, M. *J. Phys. Chem. B* **2005**, *109*, 11622.
(17) Ferrin, P.; Nilekar, A. U.; Greeley, J.; Rossmeisl, J.; Mavrikakis, M. *Surf. Sci.* **2008**, *602*, 3424.
(18) Greeley, J.; Jaramillo, T. F.; Bonde, J.; Chorkendorff, I. B.; Nørskov, J. K. *Nat. Mater.* **2006**, *5*, 909.
(19) Nilekar, A. U.; Xu, Y.; Zhang, J. L.; Vukmirovic, M. B.; Sasaki, K.; Adzic, R. R.; Mavrikakis, M. *Top. Catal.* **2007**, *46*, 276.
(20) Gu, Z. H.; Balbuena, P. B. *J. Phys. Chem. A* **2006**, *110*, 9783.
(21) Greeley, J.; Nørskov, J. K. *Electrochim. Acta* **2007**, *52*, 5829.
(22) Jarvi, T. D.; Sriramulu, S.; Stuve, E. M. *Colloids Surf., A* **1998**, *134*, 145.
(23) Housmans, T. H. M.; Wonders, A. H.; Koper, M. T. M. *J. Phys. Chem. B* **2006**, *110*, 10021.
(24) Iwasita, T. *Electrochim. Acta* **2002**, *47*, 3663.
(25) Bergamaski, K.; Pinheiro, A. L. N.; Teixeira-Neto, E.; Nart, F. C. *J. Phys. Chem. B* **2006**, *110*, 19271.
(26) Frelink, T.; Visscher, W.; Vanveen, J. A. R. *J. Electroanal. Chem.* **1995**, *382*, 65.
(27) Hammer, B.; Hansen, L. B.; Nørskov, J. K. *Phys. Rev. B* **1999**, *59*, 7413.
(28) Greeley, J.; Nørskov, J. K.; Mavrikakis, M. *Annu. Rev. Phys. Chem.* **2002**, *53*, 319.
(29) Neugebauer, J.; Scheffler, M. *Phys. Rev. B* **1992**, *46*, 16067 LP.
(30) Bengtsson, L. *Phys. Rev. B* **1999**, *59*, 12301.
(31) Vanderbilt, D. *Phys. Rev. B* **1990**, *41*, 7892.
(32) Monkhorst, H. J.; Pack, J. D. *Phys. Rev. B* **1976**, *13*, 5188.

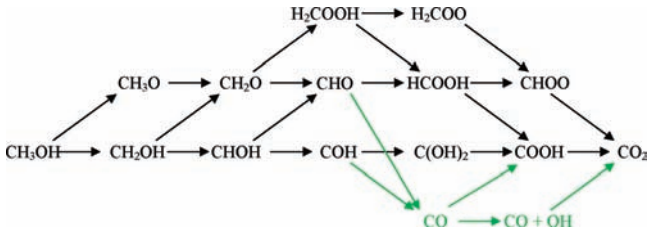

Figure 1. Schematic representation of the reaction paths and possible intermediates considered here for methanol electrooxidation. Green arrows indicate the indirect mechanism to CO_2 formation. Arrows to the right also include the generation of a proton/electron pair (not shown) from either the carbonaceous species or the surrounding H_2O (the latter implies the addition of a hydroxyl group). We note that liquid-phase reactions can take place for CH_2O and HCOOH, but are not included in our analysis.[23]

energies of surface intermediates are also calculated in a similar manner, for example:

$$CO_2(g) + 2H_2(g) + * \rightarrow CHOH* + H_2O(1)$$

$$\Delta G_{CHOH*} = TE_{H2O} + TE_{CHOH*} - TE_{CO2} - 2*TE_{H2} - TE_{clean} + ZPE_{H2O} + ZPE_{CHOH*} - ZPE_{CO2} - 2*ZPE_{H2} - T*(S_{H2O} + S_{CHOH*} - S_{CO2} - 2*S_{H2})$$

where TE_{clean} is the total energy of the clean slab, TE_{CHOH*} is the total energy of CHOH* adsorbed on a clean slab, ZPE_{CHOH*} and S_{CHOH*} are the zero-point energy and entropy for the adsorbed CHOH*, and the rest of the terms are as defined above.

To treat the electrochemical potential (U), we apply the concept of the computational standard hydrogen electrode (SHE).[12] For this reference, under standard conditions, the free energy of two protons and two electrons at zero potential is equal to the free energy of the hydrogen molecule. The change in free energy at a given potential U of a reaction involving the formation of a proton electron pair versus that at the SHE is equivalent to $\Delta G = -eU$, where e is the charge on the electron. This approach has been used to successfully describe several other reactions; further details can be found therein.[12,36−38]

Using this concept, we can calculate the onset potential and reaction pathway of methanol electrooxidation in the following manner. Given that an applied potential U will change the free energy of all electrons by $\Delta G = -eU$, if one looks at the overall reaction mechanism (Figure 1), on any catalytic surface, there exists a potential at which the free energy of all reaction steps along at least one oxidative pathway becomes exothermic in the product direction. We define this potential as the onset potential of the reaction. Mathematically, this is defined as:

$$U_{onset} = \min\left(\max\left(\frac{\Delta G^i_{SHE}}{e}\right)\right)_j$$

where i refers to steps along a given pathway, j is the set of all possible pathways, ΔG_{SHE} is the change in free energy for the reaction step at 0 V versus SHE, e is the charge on an electron, and U_{onset} is the onset potential. One can also use this information to define the possible reaction pathway at the onset potential. Furthermore, the most endothermic step along this pathway is defined as the potential-determining step, as it defines what the onset potential will be on a given catalytic surface. Yet, we note here that while at $U = U_{onset}$, methanol electrooxidation is thermodynamically feasible, kinetics and surface poisoning may render the activity of the catalyst very low at this potential.

Results and Discussion

The overall anode reaction for direct methanol fuel cells is:

$$CH_3OH + H_2O \rightarrow CO_2 + 6H^+ + 6e^-$$

This reaction can follow multiple pathways; in the present analysis, we restrict ourselves to possible intermediates occurring in proton- and electron-transfer reactions. Additionally, we consider only Heyrovsky-type reactions,[39] except in the case of adsorbed CO* and OH* forming gas-phase CO_2 and a proton/electron pair, where CO−O bond formation and a Heyrovsky proton−electron transfer step occur. Importantly, we include only the thermodynamic barriers; while kinetics will play a role, we believe that the general trends described here provide a valid representation of fuel cell chemistry on different metal surfaces. Intermediates that are closed-shell molecules (e.g., CH_3OH, CO_2) are treated as gas-phase molecules, as the bond energy to the surface will be unlikely to overcome the entropy loss through surface binding. Hydrogen adsorption is not considered in our study, as at any reasonable DMFC anode potential hydrogen coverage is known to be very low.[40]

The overall reaction pathways considered in our analysis are given in Figure 1. Two broad classes of reaction mechanism are accounted for: (1) the direct mechanism, wherein methanol is oxidized to CO_2 without going through a CO* intermediate, and (2) the indirect mechanism, where CO* is a reaction intermediate. The exact pathway utilized under standard methanol electrooxidation conditions has been the subject of discussion in the literature;[16,41−44] accordingly, the role of different surfaces in selectively promoting either of these pathways is unclear. For example, several groups have asserted that at moderate potential, the reaction on Pt takes place via the direct mechanism on the (111) facet, but via the indirect mechanism on the (100) facet.[16,23] Jarvi and Stuve[22] also point to the difference in CO* poisoning of the two surfaces as indicative of possible structure sensitivity in the reaction mechanism. Unfortunately, only limited mechanistic analysis is available on facets of other transition metals.[41] The relative free energies of all reaction intermediates on the eight fcc(100) surfaces studied here are given in Table 1. These can be compared to the energetics of the same reaction intermediates on the corresponding fcc(111) surface, as reported recently[17] and also provided in Table 1. We note that a positive value in the table indicates that the surface species is not as stable as the reference molecules at the standard conditions (CO_2(g), H_2O(l), and H_2(g) at 298 K and 1 bar pressure); while these molecules can exist on the surfaces studied, reaction to form the reference molecules would be exothermic at standard conditions.

(33) Perdew, J. P.; Chevary, J. A.; Vosko, S. H.; Jackson, K. A.; Pederson, M. R.; Singh, D. J.; Fiolhais, C. *Phys. Rev. B* **1992**, *46*, 6671.
(34) Greeley, J.; Mavrikakis, M. *Surf. Sci.* **2003**, *540*, 215.
(35) *CRC Handbook of Chemistry and Physics*, 76th ed.; CRC Press: New York, 1996.
(36) Karlberg, G. S.; Rossmeisl, J.; Nørskov, J. K. *Phys. Chem. Chem. Phys.* **2007**, *9*, 5158.
(37) Rossmeisl, J.; Logadottir, A.; Nørskov, J. K. *Chem. Phys.* **2005**, *319*, 178.
(38) Rossmeisl, J.; Qu, Z. W.; Zhu, H.; Kroes, G. J.; Nørskov, J. K. *J. Electroanal. Chem.* **2007**, *607*, 83.
(39) Vetter, K. J. *Electrochemical Kinetics: Theoretical and Experimental Aspects*; Academic Press: New York, 1967.
(40) Hamnett, A. *Catal. Today* **1997**, *38*, 445.
(41) Kua, J.; Goddard, W. A. *J. Am. Chem. Soc.* **1999**, *121*, 10928.
(42) Bagotzky, V. S.; Vassiliev, Y. B.; Khazova, O. A. *J. Electroanal. Chem.* **1977**, *81*, 229.
(43) Chen, Y. X.; Miki, A.; Ye, S.; Sakai, H.; Osawa, M. *J. Am. Chem. Soc.* **2003**, *125*, 3680.
(44) Markovic, N. M.; Ross, P. N. *Surf. Sci. Rep.* **2002**, *45*, 121.

Table 1. d-Band Center with Respect to the Fermi Level ($\varepsilon_d - \varepsilon_f$) and Calculated Adsorption Free Energies (in eV) for Methanol Electrooxidation Intermediates at Standard Conditions (298 K, 1 bar) on the (111) and (100) Facets of Eight fcc Metals[a]

	facet	$\varepsilon_d - \varepsilon_f$	CH_3O	CH_2OH	CHOH	H_2COOH	CHO	COH	H_2COO	$C(OH)_2$	CO	CHOO	COOH	OH
Rh	(111)	−2.10	0.46	0.63	0.43	0.91	0.30	−0.07	1.33	0.46	−0.58	0.25	0.32	0.54
	(100)	−1.88	0.18	0.27	−0.01	0.25	−0.60	−0.55	0.16	0.14	−0.90	−0.06	−0.19	0.02
Ir	(111)	−2.92	0.72	0.51	0.47	0.91	0.32	0.01	1.36	0.25	−0.49	0.24	0.26	0.67
	(100)	−2.64	0.02	0.03	−0.30	0.27	−0.66	−0.59	0.04	−0.27	−1.05	−0.14	−0.32	−0.08
Ni	(111)	−1.59	0.27	0.96	0.80	0.67	0.53	0.21	1.25	0.92	−0.56	0.39	0.65	0.29
	(100)	−1.49	0.04	0.60	0.45	0.21	0.27	−0.12	0.66	0.56	−0.71	−0.08	0.28	−0.04
Pd	(111)	−1.86	1.08	0.63	0.70	1.28	0.46	0.26	2.42	0.65	−0.62	0.85	0.71	1.04
	(100)	−1.75	0.83	0.63	0.29	0.97	0.29	0.04	1.59	0.26	−0.62	0.65	0.40	0.70
Pt	**(111)**	**−2.48**	**1.15**	**0.41**	**0.39**	**1.24**	**0.36**	**0.05**	**2.43**	**0.14**	**−0.41**	**0.94**	**0.51**	**1.16**
	(100)	**−2.38**	**0.71**	**0.31**	**−0.18**	**0.96**	**0.18**	**−0.08**	**1.39**	**−0.04**	**−0.78**	**0.61**	**0.17**	**0.56**
Cu	(111)	−2.57	0.63	1.59	1.96	0.99	1.58	2.03	1.77	1.64	0.62	0.43	1.38	0.57
	(100)	−2.48	0.29	1.26	1.57	0.52	1.21	1.56	0.73	1.45	0.50	0.12	1.01	0.17
Ag	(111)	−4.23	1.06	1.77	2.51	1.39	1.84	3.00	2.50	1.98	1.23	0.89	1.71	0.98
	(100)	−4.17	0.70	1.64	2.17	0.96	1.71	2.76	1.65	1.92	1.02	0.50	1.45	0.53
Au	(111)	−3.45	1.82	1.39	2.18	2.11	1.50	2.57	3.42	1.56	1.23	1.41	1.55	1.71
	(100)	−3.40	1.32	1.18	1.46	1.48	1.30	1.58	2.35	1.37	0.72	1.07	1.34	1.10

[a] Entries for Pt are in bold. CO_2(g), H_2O(l), and H_2(g) are used as reference. Zero-point energy and entropy corrections are included. Calculated free energies for closed-shell gas-phase intermediates are: CH_3OH = 0.11 eV; CH_2O = 0.71 eV; HCOOH = 0.42 eV; CO_2 = 0 eV. The absolute DFT error for these molecules is reasonably small; for comparison, the standard table values are: CH_3OH(g) = 0.05 eV; CH_2O(g) = 0.57 eV; HCOOH(g) = 0.44 eV; CO_2(g) = 0 eV.

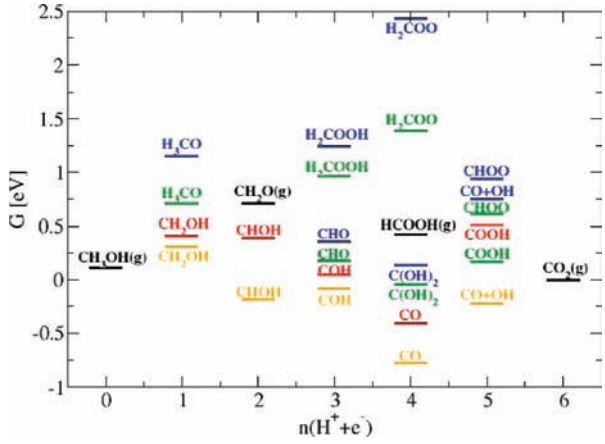

Figure 2. Free energies for all methanol electrooxidation intermediates on the Pt(111) and Pt(100) surfaces, with H_2, CO_2, and H_2O as a reference; see also Table 1. In red/orange are the most stable intermediates for each step on the (111)/(100) facet, respectively. Other isomeric intermediates with a higher energy are shown in blue/green, respectively. The energy levels of gas- and liquid-phase molecules, independent of the metal surface, are shown in black. The *x*-axis indicates how many proton/electron pairs have been created from the original reactants (e.g., $CH_3OH + H_2O \rightarrow HCOOH\ (g) + 4H^+ + 4e^-$).

Electrooxidation of Methanol on Pt(111) and Pt(100). As Pt is known to be the best monometallic catalyst for the electrooxidation of methanol,[16,45,46] we begin our analysis by looking at the differences between methanol electrooxidation on the (100) and (111) surfaces of this metal. The stability of all intermediates studied on these two surfaces is compared in Figure 2. The more open Pt(100) surface binds all intermediates more strongly than the closer-packed (111) surface. If one looks at the d-band center of the two facets (shown in Table 1), one can see that Pt(100) has a d-center closer to the Fermi level than the Pt(111) surface, which would explain the higher reactivity of the surface.[47] This result is not surprising, given the lower coordination of the (100) surface atoms (each surface atom has eight nearest neighbors as compared to nine on the (111) surface; bulk fcc metal atoms have 12 nearest neighbors).[48] One can calculate the onset potential for the overall chemical reaction for each metal on both the (100) and the (111) surfaces (see Figure 3). For Pt, the onset potential of the direct mechanism is somewhat lower on the (100) surface (0.37 V on (111) versus 0.21 V on (100)). The indirect (via CO*) mechanism is significantly easier on the (100) surface (0.56 V vs 0.92 V on the (111) surface). This large difference in the indirect mechanism is a result of the much stronger binding of OH*, and therefore the much more accessible water activation, on the (100) facet as compared to the (111) facet. Because of the very strong binding of CO* on the (100) surface (much stronger than the binding on the (111) surface), the activity of methanol electrooxidation through the direct mechanism on the (100) surface will be very low due to CO* poisoning of the surface; however, the formation of CO_2 via the direct mechanism at low potentials has been noted on this surface at relatively low potentials.[49−51] At intermediate potentials ($U \approx 0.6$ V), both the direct and the indirect pathways are thermodynamically available on Pt(100), whereas on Pt(111) only the direct pathway is available. Given the high CO* coverage that is likely to be present on both surfaces (due to that intermediates' stability), the energetic availability of the indirect pathway on Pt(100) at intermediate potentials may also account for its higher reactivity than that of Pt(111) at such potentials, as the indirect pathway allows for the removal of the CO* poison. This is consistent with the experimental and theoretical observations of Cao et al.,[16] who found that the direct pathway accounted for the activity at intermediate potentials on Pt(111) but that the indirect pathway is dominant on Pt(100) at these potentials. At higher potentials, we predict that the indirect pathway becomes available to Pt(111) as well. This is in line with experiments, which find that at these potentials, the activity of the two surfaces is very similar.[22] A direct quantitative comparison

(45) Greeley, J.; Mavrikakis, M. *J. Am. Chem. Soc.* **2004**, *126*, 3910.
(46) Greeley, J.; Mavrikakis, M. *J. Am. Chem. Soc.* **2002**, *124*, 7193.
(47) Mavrikakis, M.; Hammer, B.; Nørskov, J. K. *Phys. Rev. Lett.* **1998**, *81*, 2819.
(48) Jiang, T.; Mowbray, D. J.; Dobrin, S.; Falsig, H.; Hvolbaek, B.; Bligaard, T.; Nørskov, J. K. *J. Phys. Chem. C* **2009**, *113*, 10548.
(49) Jarvi, T. D.; Sriramulu, S.; Stuve, E. M. *J. Phys. Chem. B* **1997**, *101*, 3649.
(50) Herrero, E.; Chrzanowski, W.; Wieckowski, A. *J. Phys. Chem.* **1995**, *99*, 10423.
(51) Herrero, E.; Franaszczuk, K.; Wieckowski, A. *J. Phys. Chem.* **1994**, *98*, 5074.

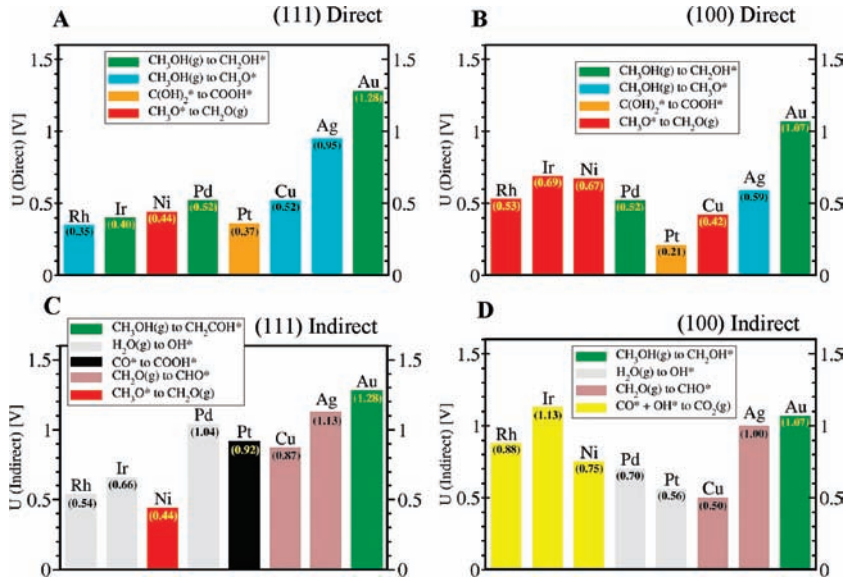

Figure 3. The onset potential and potential-determining steps for methanol electrooxidation via the direct and indirect mechanisms on the (111) and (100) facets of 8 transition metals. (A) Direct mechanism, (111) facet. (B) Direct mechanism, (100) facet. (C) Indirect (via CO*) mechanism, (111) facet. (D) Indirect (via CO*) mechanism, (100) facet. The color of each bar indicates the potential-determining step, as explained in each legend.

between model and experiments is beyond the scope of this work, due to kinetic, diffusion, coverage, solvent, and other effects not included in this simple model. However, we believe our model is adequate for capturing trends in reactivity across surfaces, as discussed here.

Methanol Electrooxidation on (111) and (100) Surfaces of Other Transition Metals. We can also extend this analysis to other metals to examine the trends in structure sensitivity across transition metals. The free energies of adsorption for the selected surface intermediates on both the (111) and the (100) facets of eight transition metals are given in Table 1. A comparison of the onset potential for the direct and indirect mechanisms on these surfaces is shown in Figure 3. The pathway and potential-determining step for the direct and indirect mechanism on the (100) and (111) surface of each transition metal are shown in Figure 4.

Direct Mechanism. For the transition metals studied, almost all surface species are bound more strongly on the (100) than on the (111) surface (CO* and H_2COH* have the same free energy on Pd(111) and Pd(100)). As noted previously, this higher reactivity for the more open surfaces is in line with the upshift in the d-band center for the more open surface as compared to the (111) surface and, therefore, is of electronic origin (see Table 1). As a result, reaction steps involving the transformation of a gas-phase species to a surface species are more exothermic on the more open surface; conversely, steps involving the formation of a closed-shell molecule will be energetically more difficult on the more-open surface. Consequently, for the three group 11 metals (Au, Ag, Cu) and the direct mechanism, where initial H abstraction from methanol is the onset-potential determining step (PDS) on the (111) surface, the onset potential is much lower on the (100) facet (see Figures 3A,B and 4A,B). In fact, for Cu, the increased binding results in a change in the PDS: from initial H abstraction on the (111) surface to the release of a surface species to the gas-phase on the (100) surface. On Pt, where the PDS does not involve a closed-shell molecule, the effect of facets on the ΔG of the potential-determining step is more ambiguous. On both Pt facets, the initial H abstraction requires a potential within

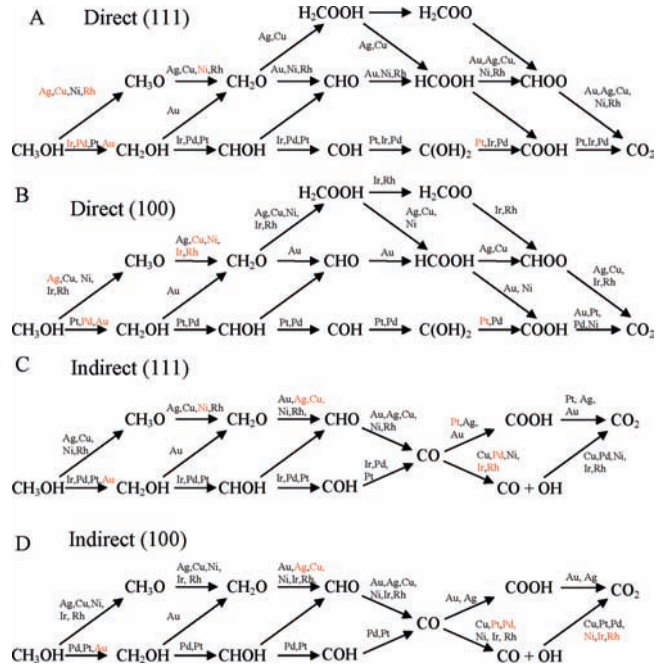

Figure 4. (A,B) The thermodynamic minimum-energy paths for methanol electrooxidation along the direct mechanism on the (111) [A] and (100) [B] facets of the metals studied, with the potential-determining step indicated in red for each metal. (C,D) The thermodynamic minimum-energy paths for methanol electrooxidation considering only the indirect mechanism on the (111) [C] and (100) [D] facets of the metals studied, with the potential-determining step indicated in red for each metal. Arrows with no metal name indicated on them were considered as possible steps but are found not to be thermodynamically favorable for any of the metals studied.

0.1 V of the reported PDS. As with the group 11 metals, initial H abstraction is easier on the more open (100) surface of Pt. For the direct mechanism, on Rh, Ir, and Ni, the (111) surface has a lower onset potential than the (100) surface. In the case of Rh and Ir, the potential-determining step on the more close-packed surface is the initial H abstraction; this becomes easier on the (100) surface due to the stronger bonding; however, the release of the surface intermediates becomes more difficult, and

thus the onset potential is much higher on the open surface. In the case of Ni, even on the (111) facet the PDS is the transformation of a surface species to a closed-shell species; as expected, this can be accomplished at a much lower potential on the weaker-binding (111) surface than on the (100) surface. Pd is an exception; the initial hydrogen abstraction to form CH_2OH^* is equally difficult on both facets, and thus there is no change in PDS or onset potential between the two Pd facets considered.

Indirect Mechanism. As shown in Figure 3, on both the (111) and the (100) surfaces for every metal, the indirect mechanism has an onset potential equal to or greater than the onset potential characterizing the direct mechanism. Figure 4C and D shows the mechanism and potential-determining step for methanol electrooxidation along the indirect pathways for these metals. The trend in onset potential for the indirect mechanism for different facets of the same metal is very similar to that found for the direct mechanism. As with the direct mechanism, for the indirect mechanism Rh, Ir, and Ni show a higher onset potential on the more-open (100) surface than the close-packed (111) surface. For the indirect mechanism on these metals, there is a change in the PDS between the two surfaces studied. On the (111) surfaces, water activation for Rh and Ir is the PDS; on Ni, it is the removal of methoxy. Because of the stronger binding of all species on the (100) surfaces, the H abstraction becomes easier, but poisoning the surface by reactive intermediates becomes a problem. On Rh(100), Ir(100), and Ni(100), removal of OH* and CO*, due to their too-strong binding, is the PDS (see Figure 3D). In contrast to these three metals, on Pt and Pd the onset potential is much lower on the open surface than the close-packed one, because of the much stronger binding of OH* on the Pt and Pd(100) surfaces (G_{OH^*} of 0.70 and 0.56 eV for Pd(100) and Pt(100) as compared to G_{OH^*} of 1.04 and 1.16 eV on the respective (111) surfaces). This stronger binding allows for much easier water activation on the (100) surface. As water activation (either directly or through carboxyl formation) is the PDS for the indirect pathway on both facets of Pt and Pd, the more facile H_2O activation on the open surface results in a lower onset potential. For group 11 metals, stronger binding of species on the (100) surface as compared to the (111) surface makes dehydrogenation reactions (H abstraction from methanol for Au; H abstraction from H_2CO for Cu and Ag) much more favorable at low potentials on the (100) surface than on the (111) surface.

Structure Sensitivity. By comparing the onset potential of the direct and indirect mechanisms on different facets of the same metal (as in Figure 3), one may derive information on the structure sensitivity of methanol electrooxidation on each metal. We note that, to our knowledge, systematic experimental studies have not been performed to determine the structure sensitivity of methanol electrooxidation on metals other than Pt. On Au, the onset potential for both mechanisms on both facets is extremely high, although significantly higher for the (111) facet than the (100) facet. On Ag, there is a possibility of reaction occurring through the direct mechanism on the (100) facet at intermediate potentials ($U \approx 0.6$ V); on neither facet is the indirect mechanism competitive. On Cu(100), the indirect and direct mechanisms have similar onset potential, although different PDS. In contrast, on Cu(111), the direct mechanism has an onset potential clearly lower than the indirect mechanism, and the PDS for the two mechanisms is different. As noted previously, the difference in onset potential on Pt for the indirect mechanism between the (100) and (111) facets will lead to dominance of that pathway on the more-open facet at intermediate potentials, while the relative ease of the direct pathway for both facets at low potentials allows methanol electrooxidation at such potentials even on the (111) surface. On Pd(100), the direct mechanism has a lower onset potential than the indirect mechanism. On Pd(111), the indirect mechanism is not competitive at all. Yet, the nature of the PDS remains invariant with Pd facet for both the direct and the indirect mechanism. On Rh and Ir, the direct mechanism has a much lower onset potential than does the indirect mechanism for both facets. On Ni, the indirect and direct pathways have similar onset potentials on each surface, but clearly the onset potential is higher on the (100) facet than it is on the (111) facet, a signature of structure sensitivity.

The origin of this structure sensitivity can be understood in the stronger binding of all intermediates on the less-coordinated sites of the (100) surface as compared to the (111) surface.[48,47] For metals where the potential-determining step for methanol electrooxidation is the formation of surface species (e.g., Au), the stronger binding leads to a lower onset potential on the (100) surface. For more reactive metals (e.g., Ni), where the potential-determining step is the removal of a surface species from the surface, the close-packed (111) surface will have a lower onset potential, as the adsorbates can more easily be removed from that surface.

Reactivity Descriptors for Methanol Electrooxidation. Direct Mechanism. In a recent paper,[17] we demonstrated that the free energy of molecules adsorbed through carbon is linearly correlated with the free energy of adsorbed carbon monoxide (CO*) on the (111)/(0001) surface of transition metals. Additionally, the free energy of molecules bound through oxygen is linearly correlated with the free energy of surface hydroxyl (OH*). This correlation between adsorbate binding can be understood through the following model: Adsorption on a transition metal surface can be understood as the interaction of two types of transition metal electron states, the hybridized *sp* states and the *d* states of the metal, with the adsorbate *sp* hybridized states. Across transition metals, there is very little variation in the *sp* states; thus variation in the d states accounts for much of the difference in adsorption strength across transition metals. The interaction of the *d* states and the *sp* states of any given adsorbate, therefore, determines relative bond strength on different metals. Because this is true of all adsorbates bound through the same atom (e.g., OH* and CH_3O^*), they are also linearly correlated with each other. The slopes for the correlation of different adsorbates can be understood through the differences in generalized bond order of the adsorbed atom. For a more detailed explanation, we refer the reader to Abild-Pedersen et al.[52] and references therein.[53] Here, we find that a similar scaling exists (with different correlations) between species bound to the (100) surface of transition metals. The different correlations for the two surface terminations are not surprising, given the different adsorption geometries and sites on the different surfaces.[52] Thus, we can describe methanol electrooxidation on the (100) surface using the same two key reactivity descriptors derived for the (111)/(0001) surfaces, G_{CO^*} and G_{OH^*}. A selection of the correlations for individual steps and reaction intermediates on the (100) surface is given below (all correlations are provided in the Supporting Information).

(52) Abild-Pedersen, F.; Greeley, J.; Studt, F.; Rossmeisl, J.; Munter, T. R.; Moses, P. G.; Skulason, E.; Bligaard, T.; Nørskov, J. K. *Phys. Rev. Lett.* **2007**, *99*, 016105.
(53) Bell, A. T.; Shustorovich, E. *J. Catal.* **1990**, *121*, 1.

The respective correlations on the (111)/(0001) surfaces are taken from ref 17. The correlations on the (100) surface are:

$$CH_3OH(g) \rightarrow CH_2OH^* + H^+ + e^-$$
$$G_{CH2OH^*} = 0.66^*G_{CO^*} + 0.89\ \text{eV}$$
$$\Delta G = 0.66^*G_{CO^*} + 0.78\ \text{eV}$$

$$CH_3OH(g) \rightarrow CH_3O^* + H^+ + e^-$$
$$G_{CH3O^*} = 1.08^*G_{OH^*} + 0.11\ \text{eV}$$
$$\Delta G = 1.08^*G_{OH^*}$$

$$CH_2OH^* \rightarrow CH_2O(g) + H^+ + e^-$$
$$G_{CH2OH^*} = 0.66^*G_{CO^*} + 0.89\ \text{eV}$$
$$\Delta G = -0.66^*G_{CO^*} - 0.18\ \text{eV}$$

$$CH_2O(g) \rightarrow CH_2OOH^* + H^+ + e^-$$
$$G_{CH2OOH^*} = 1.08^*G_{OH^*} + 0.30\ \text{eV}$$
$$\Delta G = 1.08^*G_{CO^*} - 0.41\ \text{eV}$$

$$CH_3O^* \rightarrow CH_2O(g) + H^+ + e^-$$
$$G_{CH3O^*} = 1.08^*G_{OH^*} + 0.11\ \text{eV}$$
$$\Delta G = -1.08^*G_{OH^*} + 0.60\ \text{eV}$$

$$CHO^* \rightarrow HCOOH(g) + H^+ + e^-$$
$$G_{CHO^*} = 1.01^*G_{CO^*} + 0.69\ \text{eV}$$
$$\Delta G = -1.01^*G_{CO^*} - 0.27\ \text{eV}$$

The above analysis suggests that the adsorption free energies of CO* (G_{CO^*}) and OH* (G_{OH^*}) are two key descriptors for the overall reaction scheme shown in Figure 1 and that these quantities can be used to estimate the adsorption free energies for all other reaction intermediates implicated in the direct and indirect mechanism. This allows us to get a simplified overview of the reaction mechanism. The two-dimensional phase-space generated by the continuous variation of these two parameters is mapped out in Figure 5, where the different regimes (shown as a function of G_{CO^*} and G_{OH^*}) correspond to particular potential-determining steps and are labeled accordingly. The lines in Figure 5 represent the border between two regimes with different potential-determining step. Figure 5 also illustrates the compromises necessary to have a low onset potential. The lowest onset potential for the direct mechanism on both surfaces occurs at moderate OH* binding. On the (111) surface, Rh and Ni have good binding properties required for a low onset potential; for the (100) surface, Cu and Pt have very good binding characteristics for low onset potential along the direct mechanism. We stress that the reaction onset potential is only one important parameter in determining the efficiency of a fuel cell. For a highly active electrocatalyst, it is also important to avoid CO* poisoning. In this respect, metals farther to the right (higher G_{CO^*}) are better. Additionally, many metals oxidize or dissolve[21] under electrochemical conditions, rendering them unfit for use as DMFC anode catalysts.

It is instructive to note the differences in the phase-spaces in the direct mechanism on the two facets studied (panels A and B in Figure 5). While the same potential-determining steps are mapped by the phase-spaces on both facets, the lowest-onset-potential region on the (100) surface is lower in G_{OH^*}, while slightly higher in G_{CO^*}. If one were to superimpose the isopotential spaces of the two surfaces, the boundaries between different potential-determining steps (shown in Figure 5) would be shifted down and to the right for the (100) surface as compared to the (111) surface.

Indirect Mechanism. A similar examination of the indirect mechanism is also of value, for the following reasons. First, as explained above, multiple groups have speculated on the existence of the indirect mechanism, at least on some facets of the Pt surface. Second, an efficient anode for direct methanol fuel cells will have to address the problem of CO* poisoning. By allowing any CO* generated through decomposition of methanol to completely oxidize, one can alleviate the latter problem. Using a similar analysis to the one described above, we employ the linear scaling relationships to map out the indirect mechanism phase-space. Selected correlations applicable to the indirect mechanism on the (100) facet are given below; those for the (111) facet are taken from ref 17. The correlations on the (100) surface are:

$$CH_3OH(g) \rightarrow CH_2OH^* + H^+ + e^-$$
$$G_{CH2OH^*} = 0.66^*G_{CO^*} + 0.89\ \text{eV}$$
$$\Delta G = 0.66^*G_{CO^*} + 0.78\ \text{eV}$$

$$CH_3OH(g) \rightarrow CH_3O^* + H^+ + e^-$$
$$G_{CH3O^*} = 1.08^*G_{OH^*} + 0.11\ \text{eV}$$
$$\Delta G = 1.08^*G_{OH^*}$$

$$CH_3O^* \rightarrow CH_2O(g) + H^+ + e^-$$
$$G_{CH3O^*} = 1.08^*G_{OH^*} + 0.11\ \text{eV}$$
$$\Delta G = -1.08^*G_{OH^*} + 0.60\ \text{eV}$$

$$CH_2O(g) \rightarrow CHO^* + H^+ + e^-$$
$$G_{CHO^*} = 1.01^*G_{CO^*} + 0.69\ \text{eV}$$
$$\Delta G = 1.01^*G_{CO^*} - 0.02\ \text{eV}$$

$$H_2O(l) \rightarrow OH^* + H^+ + e^-$$
$$\Delta G = G_{OH^*}$$

$$CO^* + OH^* \rightarrow CO_2(g) + H^+ + e^-$$
$$\Delta G = -G_{CO^*} - G_{OH^*}$$

$$CO^* \rightarrow COOH^* + H^+ + e^-$$
$$G_{COOH^*} = 0.80^*G_{CO^*} + 0.70\ \text{eV}$$
$$\Delta G = -0.20^*G_{CO^*} + 0.70\ \text{eV}$$

The phase-space for the onset potential of the indirect mechanism for both the (111) surface and the (100) surface are given in Figure 5, panels C and D, respectively. As with the direct mechanism, the general shape of the two spaces is similar. On both facets studied, for surfaces with weak CO* binding, the formation of formyl (CHO*) is potential-determining. For strong CO* binding, the oxidation of CO* is difficult. For strong OH* binding, the decomposition of adsorbed methoxy to formaldehyde is potential-determining, while weak OH* binding indicates difficulty with the activation of water, either directly or through the COOH* intermediate. Weak CO* and OH* binding indicates difficulty with initial methanol oxidation for both surfaces.

Figure 5 can also illustrate the structure sensitivity of a particular metal. The relative position of any surface on that map will depend on the CO* and OH* binding, which will vary from facet to facet for a given metal. By comparing the relative position of a metal on the map for each facet, one can predict the potential-determining step and onset potential for each facet,

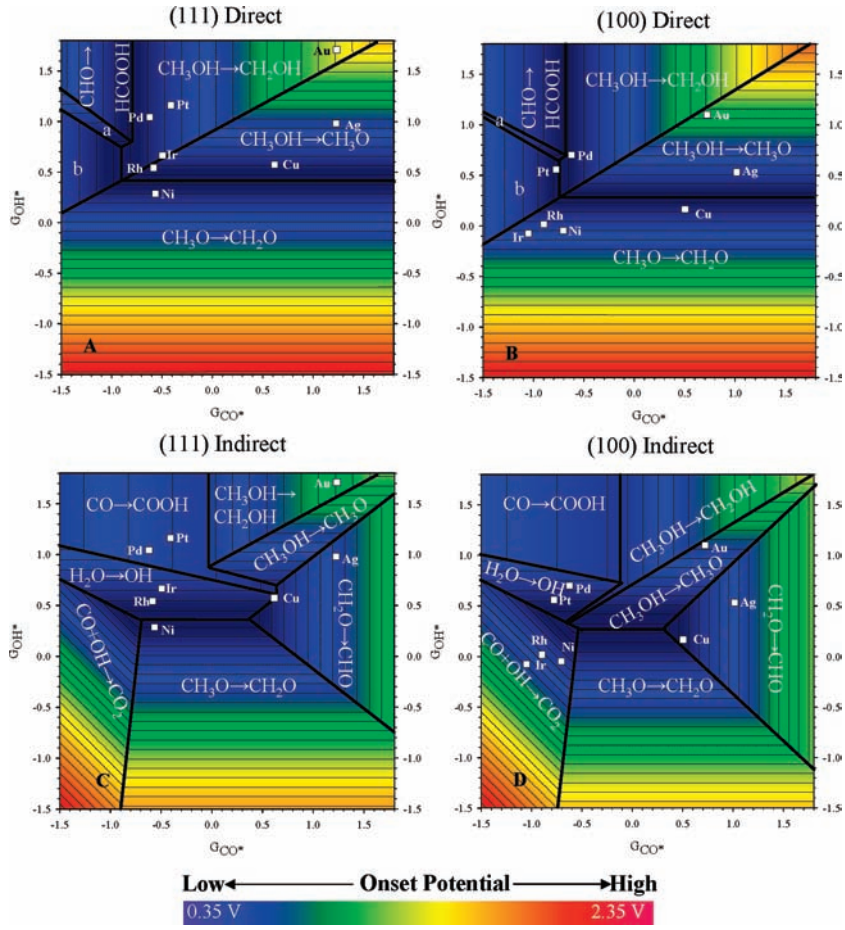

Figure 5. The potential-determining steps for methanol electrooxidation on (111) and (100) facets plotted using G_{CO*} and G_{OH*} as descriptors. (A) Direct mechanism on (111) surfaces. (B) Direct mechanism on (100) surfaces. (C) Indirect mechanism on (111) surfaces. (D) Indirect mechanism on (100) surfaces. These two adsorption free energies describe the whole reaction landscape and can be used to estimate the potential through the linear relations described in the text. For each region, the potential-determining step (PDS) is given. For the direct mechanism, region (a) has $CH_2O \rightarrow H_2COOH$ as the PDS; the PDS for region (b) is $CH_2OH \rightarrow H_2CO$. The *x*- and *y*-axis values are in eV. Iso-potential lines are included for reference. Each line represents a difference of 0.1 V. The position of the eight metals discussed in the text is included for reference. The true PDS for all metals is accurately reflected in Figures 3 and 4. Because of the scatter in the linear relations used to make this figure, the PDS illustrated here might not be exactly accurate for a few surfaces.

allowing the nature of the structure sensitivity on that metal to be predicted.

As seen in Figure 5, multiple regions in the phase-space of the potential-energy surface are sampled by the set of eight fcc metals on the (100) surface. However, the onset potential for the indirect mechanism of the monometallic surfaces is too high for practical use in direct methanol fuel cell anodes, as illustrated in Figure 3. Thus, it is important to screen for alloy catalysts, which may have lower onset potential. The predictive capacity of this approach, then, is to quickly identify sets of metals that may have synergistic effects. Using these two descriptors, we can see that for improved performance, we should seek an alloy that has moderate binding of both CO* and OH*. In particular, Figure 5 suggests that to promote the indirect mechanism further than on Pt(100), one has to devise an alloy surface that would bind CO* weaker than Pt(100) and OH* slightly stronger than Pt(100). On (111) surfaces, the indirect mechanism has a low onset potential on Ni; yet Ni may suffer from other problems such as dissolution in the reactive environment. Thus, an alloy surface that has binding characteristics similar to those of Ni but that is more resistant to degradation should be sought. One way to get such a material is to find an alloy with a surface composed of two separate metals. Such an alloy (such as the well-known Pt−Ru alloy) would need to consist of metals with different potential-determining steps (as can be easily determined from Figure 5). This alloy would utilize a bifunctional mechanism, where one type of site can perform one difficult step (e.g., H_2O activation on Ru) and the other site can easily activate a different step (e.g., initial methanol dehydrogenation or CO oxidation, which can be done on Pt). A second model alloy system may be one with homogeneous metal surface sites, which have been electronically modified, either through strain or ligand effects, such as the so-called near-surface alloys[11,54−56] possessing the desired properties. As the present work shows, the considerable structure sensitivity in metal surfaces should also be taken into account when designing such a catalyst; the stability of different alloy crystal facets may be a determining factor in overall catalyst reactivity.

Conclusions

We have investigated the onset potential and the mechanism of methanol electrooxidation on two different facets of eight

(54) Alayoglu, S.; Nilekar, A. U.; Mavrikakis, M.; Eichhorn, B. *Nat. Mater.* **2008**, *7*, 333.
(55) Zhang, J. L.; Vukmirovic, M. B.; Sasaki, K.; Nilekar, A. U.; Mavrikakis, M.; Adzic, R. R. *J. Am. Chem. Soc.* **2005**, *127*, 12480.
(56) Zhang, J. L.; Vukmirovic, M. B.; Xu, Y.; Mavrikakis, M.; Adzic, R. R. *Angew. Chem., Int. Ed.* **2005**, *44*, 2132.

fcc metals: Au, Ag, Cu, Pt, Pd, Ni, Ir, and Rh, using self-consistent, periodic density functional theory. We find significant structure sensitivity in both the onset potential of this reaction and the mechanism by which this reaction takes place. In the well-studied case of Pt, we find that on Pt(111) only the direct mechanism is thermodynamically favored at low potentials; the indirect mechanism has a much higher onset potential on that facet. Conversely, on Pt(100) both the direct and the indirect mechanisms are thermodynamically feasible at relatively low potentials. However, CO* poisoning will be much stronger on the Pt(100) facet, making the activity through the direct mechanism difficult to detect. This explains the structure sensitivity observed in experiments, whereby at intermediate potentials the indirect mechanism dominates Pt(100) activity but the direct mechanism is the only one active on Pt(111) for methanol electrooxidation. In general, for most metals studied, we predict that the indirect mechanism would have higher onset potential than the direct mechanism, on both (111) and (100) facets. For the direct mechanism, Rh, Ir, and Ni show a lower onset potential on (111), whereas Pt, Cu, Ag, and Au possess lower onset potential on the (100) facet. Pd(100) and Pd(111) show the same onset potential for the direct mechanism. Ni(111) and Au (both facets) are the two cases where direct and indirect mechanisms have the same onset potential. The origin of the calculated onset potential is directly related to the stronger binding of all intermediates on the more open (100) surface as compared to the (111) surface, which can be explained by the differences in the electronic structure and coordination of the respective surface atoms.

Additionally, we have shown that the adsorption free energies of OH* and CO* can determine the onset potential of methanol electrooxidation for a generalized fcc(100) and fcc(111) surface. Using these two reactivity descriptors, one can target an alloy surface with desirable properties for the direct methanol fuel cell anode reaction, specifically that with a low overpotential.

Acknowledgment. We gratefully acknowledge financial support from DOE-BES, Division of Chemical Sciences, and from the University of Wisconsin. Research was performed in part using supercomputing resources from the following institutions: EMSL, a national scientific user facility at Pacific Northwest National Laboratory (PNNL); the Center for Nanoscale Materials at Argonne National Laboratory (ANL); the National Center for Computational Sciences at Oak Ridge National Laboratory (ORNL); and the National Energy Research Scientific Computing Center (NERSC). EMSL is sponsored by the Department of Energy's Office of Biological and Environmental Research located at PNNL. CNM, NCCS, and ORNL are supported by the U.S. Department of Energy, Office of Science, under contract nos. DE-AC02-06CH11357, DE-AC05-00OR22725, and DE-AC02-05CH11231, respectively.

Supporting Information Available: (1) Selected geometric parameters and calculated vibrational frequencies for adsorbed intermediates resulting from methanol decomposition on Pt(100); (2) binding energy of methanol decomposition intermediates on the (111) and (100) facets of eight transition metals at 1/9 ML coverage; and (3) scaling relations for the adsorption free energy of several reaction intermediates bound through O or C to the metal surfaces. This material is available free of charge via the Internet at http://pubs.acs.org.

JA904010U